https://doi.org/10.53964/mltp.2023009

https://www.innovationforever.com

Modern
Low Temperature Plasma

ISSN 2788-807X (Online)

Open Access

Research Article

Experimental Investigation on the Effect of "Linear-Rise" Amplitude Modulation on a Pulsed Capacitively Coupled Radio-frequency Argon Discharge

Xian Zhang[1], Yanyan Fu[1], Yongxin Liu[1*]

[1]Key Laboratory of Materials Modification by Laser, Ion, and Electron Beams (Ministry of Education), School of Physics, Dalian University of Technology, Dalian, Liaoning Province, China

[*]**Correspondence to: Yongxin Liu**, PhD, Professor, Key Laboratory of Materials Modification by Laser, Ion, and Electron Beams (Ministry of Education), School of Physics, Dalian University of Technology, No. 2 Linggong Road, Ganjingzi District, Dalian, 116024, Liaoning Province, China; E-mail: yxliu129@dlut.edu.cn

Received: August 1,2023 **Revised:** October 16, 2023 **Accepted:** October 23, 2023 **Published:** December 30, 2023

Abstract

Objective: This work focused on the effect of "linear-rise" amplitude modulated waveform on the time evolution of some typical electrical and plasma parameters in a pulsed radio-frequency capacitively coupled argon discharge.

Methods: The pulse-on phase of a square wave pulse is divided into two distinct stages, namely, the "linear rise" phase (T_1 phase) and "constant amplitude" phase (T_2 phase). The study focused on exploring the impact of varying T_1 durations on the temporal evolutions of these parameters. In the experiment, the electron density was measured time-resolved by a hairpin probe. Phase-resolved optical emission spectroscopy was employed to determine the spatial-temporal distribution of the electron impact excitation dynamics. Additionally, we determined the amplitudes and the relative phase of the discharge voltage and current, as well as the power deposition by analyzing the waveforms obtained from a voltage and a current probe.

Results: It was found that with the increase of T_1, the critical voltage value required for the plasma ignition becomes lower, and the RF power and the light intensity overshoot less significantly. Upon the overshoot, the plasma when the light intensity exhibits the maximum is dominated by the "overshoot" mode. After the pulse is turned off, the electron density under different T_1 durations first decreases with the same rate, and then the decay rate is decreased with the increase of T_1. This is because for a longer T_1, the neutral gas temperature gets lower, leading to a higher density of neutral gas, so the electron diffusion loss is suppressed.

Conclusion: Compared to the square pulse modulated radio frequency capacitively coupled plasmas, the "linear rise" amplitude modulation approach introduces external control knobs to modulate the plasma parameters, which benefits practical material processing. This paper is an experimental measurement implemented in an electropositive gas Ar discharge, and is expected to be extended to the plasmas operated in complex electronegative gases in the future.

Keywords: "linear-rise" amplitude modulation, capacitively coupled plasma, multi-fold experimental diagnostics

https://doi.org/10.53964/mltp.2023009

Citation: Zhang X, Fu YY, Liu YX. Experimental Investigation on the Effect of "Linear-Rise" Amplitude Modulation on a Pulsed Capacitively Coupled Radio-frequency Argon Discharge. *Mod Low Temp Plasma*, 2023; 1: 9. DOI: 10.53964/mltp.2023009.

1 INTRODUCTION

Low-pressure radio frequency capacitively coupled plasmas (RF-CCP) are widely used in the processing of microelectronic materials, such as etching and thin film deposition[1-5]. With the transformation of semiconductor device structures from two-dimensional to three-dimensional, etching with high depth-to-width ratio has become one of the most significant goals in semiconductor fabrication. Achieving these goals sets a higher requirement for plasma etching process, e.g., higher selectivity[6-8], anisotropic etching[9-11], and low dielectric damage, etc[12]. Ions in a continuous wave (CW) excited plasma continuously bombard the wafer surface, making it difficult to achieve these goals due to possible plasma-induced dielectric damage. It has been shown that a pulsed plasma has the potential to achieve these goals given above[13-16], due to the fact that pulsed modulated RF-CCPs have additional tuning parameters that can be used to improve the flexibility of the process by adjusting the pulse repetition frequency, duty cycle, and pulse shape[17-19]. Therefore, the study on pulsed plasmas can improve the basic understanding of the discharge mechanism and help find more suitable tuning parameters for its application in practical processes.

The complex properties exhibited by the plasma throughout the pulse period have been a topic of interest. Mishra et al.[20] conducted time-resolved measurement of plasma potential using an electron emission probe in a pulse-modulated dual-frequency capacitively coupled plasma discharge. Their findings revealed that the plasma potential aligns with the source discharge pulse voltage, maintaining positive values throughout the pulse cycle. They also observed that the CW RF bias of the substrate exerts a notable influence on the time evolution of the plasma potential. Sirse et al.[21] employed a floating hairpin probe to measure the time-dependent evolution of electron density throughout the pulse cycle in pulsed dual-frequency Ar and $Ar/O_2/CF_4$ mixed gas discharges. Their study investigated the effects of low- and high-frequency power, gas pressure, pulse repetition frequency, and duty cycle on the electron density. Experimental results demonstrated that the low-frequency power significantly affects the plasma density decay time and its absolute value, especially at lower high-frequency source power levels. Decreasing gas pressure substantially shortens the density decay time, while the choice of duty cycle and pulse repetition frequency significantly alters the time when the plasma density overshoots. Liu et al.[22] examined the impact of various discharge parameters on plasma properties in pulse-modulated RF-CCP Ar discharges using a fluid model. They observed that increasing applied voltage or electrode spacing leads to an increase in RF cycle-averaged parameters such as particle density, electric field, and electron temperature. Anjum and Rehman[17] investigated the effect of the gas pressure and the O_2 content on the evolution of plasma parameters (electron density, electron temperature, plasma potential, etc.) with time in a pulse-modulated CCP in Ar/O_2 mixed gas using RF-compensated Langmuir probes. At a gas pressure of 0.4 mbar, the electron density is lower compared to the electron density at 0.2 mbar. Furthermore, as the O_2 content increases, the electron density shows a decreasing trend. Peterson et al.[23] acquired time-resolved electron temperatures in pulse-modulated RF-CCP discharges using a hairpin resonance probe. They found that when the effective electron-neutral collision frequency is of the order of GHz, time-resolved measurement on the nanosecond scale becomes feasible. Moreover, the effective collision frequency is linked to the electron energy distribution via the effective conductivity. Thus the electron temperature can be determined by solving a set of equations that take into account these relationships.

Recently, Cho et al.[24] examined the etching characteristics of silica in pulsed CCPs under different conditions by experimental diagnostics. Their investigation revealed that the etching rate of silica increases with rising RF power and self-bias voltage. Furthermore, the presence of power on / off neutralization of negative ions on the wafer surface eradicates the occurrence of the micro-groove phenomenon. While extensive research had been conducted on pulse-modulated RF-CCP throughout the entire pulse cycle, the pulse ignition phase has received relatively little attention, particularly in terms of the pulse-modulated RF-CCP, and its underlying physical mechanisms are not well understood. Hernandez et al.[25] utilized time-resolved optical emission spectroscopy to investigate the pulsed Ar plasma re-ignition process. Their study aimed to shed light on the intrinsic physical mechanisms of ignition process of a pulse-modulated RF-CCP. Liu and coworkers[26-28] examined the evolution of system impedance and electron power absorption with time during plasma re-ignition in a pulsed capacitively coupled Ar discharge, particularly focusing on the effect of the pulse-off duration[27]. They investigated the impact of different pulse-off durations on the plasma ignition process and further studied the temporal evolution of plasma and electrical parameters at various radial positions during the plasma ignition process[28]. Their recent findings revealed that the entire system exhibits diverse modes of electron power absorption during pulse ignition[26]. Shortly after the pulse is turned on, a spike in light intensity typically occurs, which becomes more prominent with the increase of the post-glow duration[27]. During the ignition phase, the most significant increases

in light intensity, power density, and current density are observed at the discharge. In contrast, the temporal evolution of electron density exhibits relatively weak spatial dependence[28].

Despite of significant advantages of pulsed plasmas compared to conventional CW plasmas, the evolving demands of large-scale integrated circuits have surpassed the capabilities of varying pulse repetition frequency and duty cycle. As a result, there is an urgent need to identify new external control parameters. Šamara et al.[29] conducted a study on pulse-modulated RF-CCP to investigate the impact of changing the pulse shape on the physical processes. Their research revealed that by adjusting the pulse modulation shape, it is possible to control the ignition and afterglow decay processes in a pulse discharge. While most studies on pulse modulated RF-CCPs have focused on varying two variables, namely, pulse repetition frequency and duty cycle, the influence of pulse shape has received relatively little attention. By modulating the amplitude of one pulse RF signal, the degree that a plasma parameter can be modulated is increased.

In this paper, the effect of "linear-rise" amplitude modulation on the time evolution of some typical electrical and plasma parameters in a pulsed RF-CCP is investigated by various experimental diagnostics. It was found that by changing the duration of the "linear-rise" phase, it is possible to control the ignition time, the critical voltage required for the ignition, and the decay rate of electron density during the afterglow period.

The structure of the paper is organized as follows: Part II provides an introduction to the experimental chamber and the experimental diagnostics. Part III presents a comprehensive analysis and discussion of the experimental findings. Finally, in Part IV the conclusions are drawn based on the experimental results.

2 EXPERIMENTAL SET-UP AND DIAGNOSTIC TECHNIQUES

Figure 1 schematically showed the setup of the pulsed CCP source and various time-resolved diagnostic systems. The plasma was generated between two circular stainless-steel parallel plate electrodes, with a diameter of 10cm, and a separation of 2.5cm. To minimize the DC self-bias voltage of the discharge, a Teflon liner surrounding the inter-electrode plasma region was adopted. Argon gas was introduced into the chamber at a controlled flow rate of 6 Standard cubic centimeters per minute and was subsequently evacuated through the gap between the lower electrode and the Teflon liner. The gas pressure within the chamber was regulated by a throttle valve located above the mechanical pump, ensuring a constant pressure of 450mTorr.

A 12.5MHz RF voltage waveform generated by an arbitrary function generator and modulated by a customized pulse amplitude is amplified by a power amplifier and applied to the lower electrode through an "L-type" matching box to drive the discharge. The upper electrode and the side wall of the chamber were grounded. A "linear rise" pulse waveform (Figure 2) was set up by a function generator. The pulse-on phase (T_{on} phase) with the duration of 100μs was divided into two intervals, T_1 interval with a linear-rise voltage amplitude and T_2 phase with a constant voltage amplitude. The pulse off phase (T_{off} phase) duration is set to be as long as 400μs. The steady-state voltage during T_2 phase was set to be 150V in this work. The matching network here was tuned to achieve optimal matching in CW mode under the same discharge conditions, and in this case the reflected power was 0.

The ICCD camera (Andor iStar) equipped with an objective lens and an interference filter is used to probe the spatial-temporally distribution of light emission intensity (at 750.4nm) of Ar-I, corresponding to the transition $Ar2p_1 \rightarrow Ar1s_2$ based on a collision radiation model[30]. To achieve time-resolved measurements, a square wave signal synchronized with the RF signal is used to trigger a pulse delay generator, whose signal further triggers the ICCD camera. The gate width is fixed to be one RF period, t_{RF}=80ns, to acquire the time-resolved optical emission intensity (OEI).

A voltage probe (Tektronix, model P6015A) and a current probe (Pearson, model 6585) were employed to monitor the waveforms of the RF voltage and current at the power feeding point. These waveforms were recorded using an oscilloscope. It should be noted that the measured RF current comprises both the interelectrode current and the stray current resulting from parallel stray capacitance. To determine the actual interelectrode (plasma) current, the stray current is subtracted with a calibration procedure described in reference[31]. By fitting the measured waveforms with fast Fourier transform[27], the voltage amplitude (V_{rf}), the current amplitude (I_{rf}), and the relative phase (φ_{vi}) between them are obtained as a function of time. Furthermore, the power deposition (P_{tot}) into the parallel-plate system is calculated using the equation $P_{tot}=0.5 \times V_{rf} \times I_{rf} \times \cos \varphi_{vi}$.

A time-resolved hairpin probe[32,33] is used to measure the electron density, n_e, at the center of the discharge (note that the lower detection limit of the hairpin probe used in this experiment is approximately $1\times10^{14}m^{-3}$). To achieve time-resolved measurements of the electron density, a microwave signal generated by a microwave source is fed to the coupling ring through a coaxial line and a power divider, the reflected signal is rectified by a Schottky diode and recorded using a multichannel oscilloscope. The time-resolved electron density is calculated by the formula $n_e(t)=(f_r^2(t)-f_0^2)/0.81$[34]. Here, $f_r(t)$ is the time-varying resonant frequency in the plasma and f_0 is the

https://doi.org/10.53964/mltp.2023009

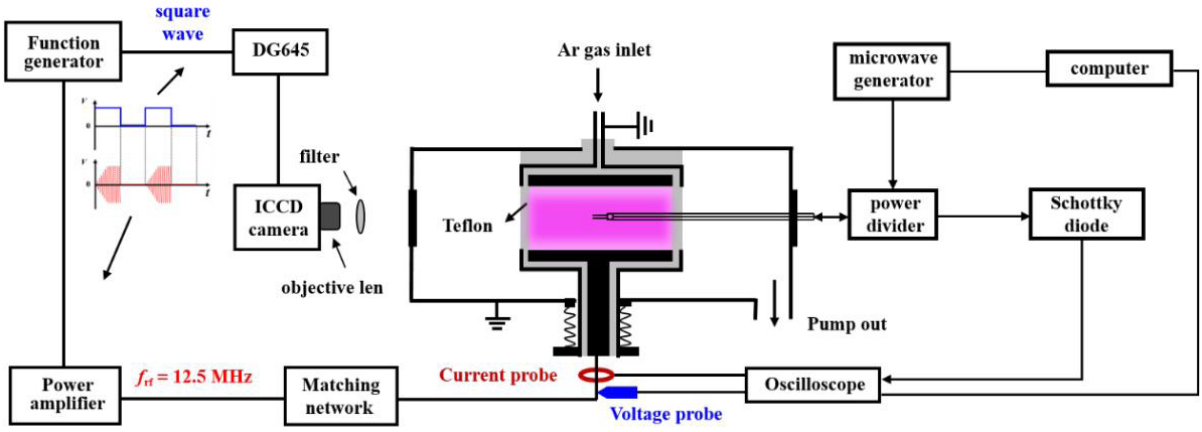

Figure 1. Schematic of pulsed CCP reactor and diagnostic methods.

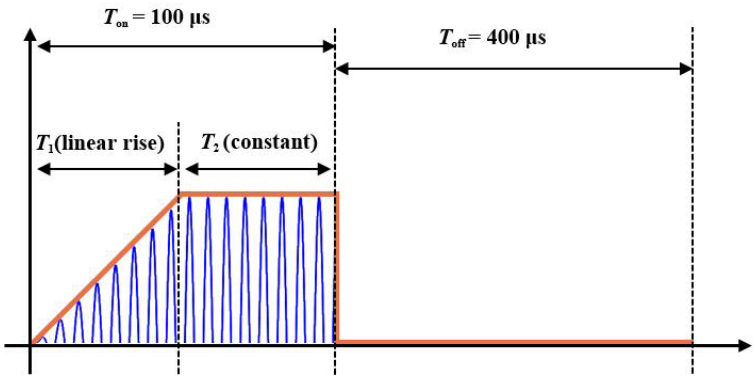

Figure 2. "Linear rise + constant" amplitude-modulated waveform. Notes: The blue line is the absolute value of the amplitude after pulse modulation, and the red line is the schematic diagram of the RF signal.

resonance frequency in vacuum, independent of time. During the measurement, the microwave source and the oscilloscope are synergistically controlled using a Labview program to ensure precise frequency scanning and data acquisition.

3 RESULTS AND DISCUSSION

This work presents an investigation about the effect of "linear-rise" amplitude modulation on the temporal evolution of various electrical parameters (the voltage amplitude, V_{rf}; the current amplitude, I_{rf}; the phase difference of the voltage and the current, φ_{vi}; and the power deposition, P_{tot}) and plasma parameters (the electron density, n_e; OEI) in a pulsed RF CCP operated under the conditions: the RF frequency, f_{rf}=12.5MHz, the gas pressure, p=450mTorr, the inter-electrode gap, L=2.5cm, and the steady-state voltage amplitude, V_{steady}=150V. The time evolution of the electrical and plasma parameters is measured and analyzed for various values of T_1 durations, i.e., T_1=5μs, 10μs, 20μs, 40μs, 60μs, and 80μs.

Figure 3 presented the time evolution of the amplitudes of V_{rf} and I_{rf} within the range of 0μs≤t≤110μs for different T_1 durations using the "linear rise + constant" amplitude modulation approach. One sees that V_{rf} and I_{rf} increase linearly, shown in Figure 3A, and then followed by a dip, indicating that the plasma ignition occurs[26,27]. By increasing T_1 duration, the growth rate of V_{rf} slowed down, and the plasma ignition was delayed. After going through the dip, V_{rf} continued to increase linearly until a steady-state value of 150V is reached. On the other hand, I_{rf} initially experienced a linear increase, followed by a more drastic growth when V_{rf} showed a dip. Afterwards, the growth of I_{rf} slowed down until it reached a steady-state value of 0.24A. It was noteworthy that the ignition onset was delayed as the T_1 duration increased, and the critical voltage required for the ignition gradually decreased. This trend persisted until T_1 exceeded 40μs, where the breakdown voltages became nearly independent of T_1. During the power-off phase, it took 10μs for V_{rf} and I_{rf} to decrease to zero after the pulse is turned off, due to the energy exchange of the inductor and capacitor in the matching network.

Figure 3C depicted the evolution of φ_{vi} within the time window of 0μs≤t≤110μs at different T_1 durations and the time evolution of V_{rf}, I_{rf}, and φ_{vi} during the first 15μs of the pulse-on period at T_1=0μs (square pulse), 5μs and 10μs under the same conditions were comparably shown in Figure 3D. It could be concluded that φ_{vi} increased from a smaller value towards 90° and then dropped to maximum

https://doi.org/10.53964/mltp.2023009

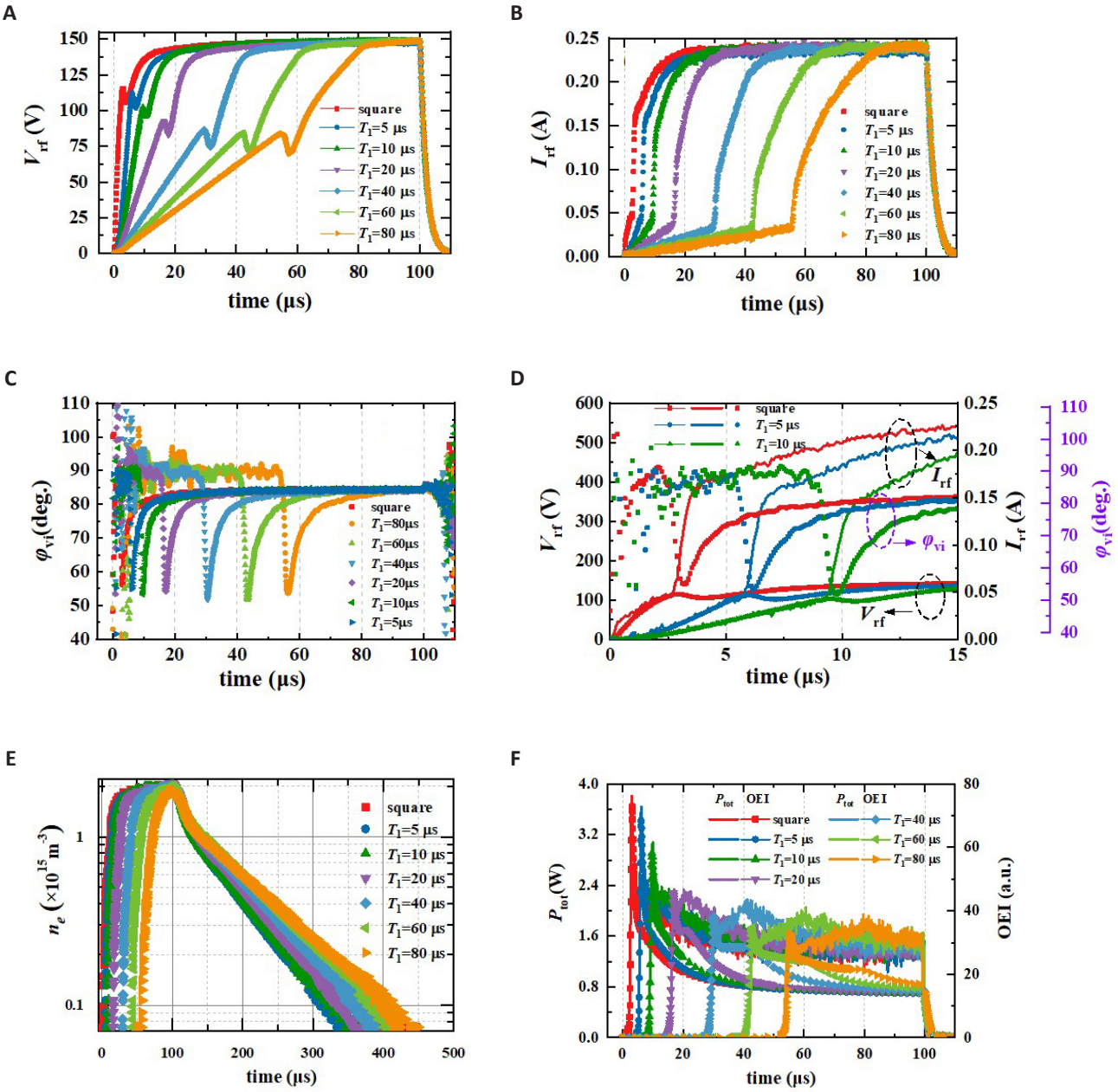

Figure 3. The diagrams of the detection parameters with time for different T_1 durations. A: The time evolution of voltage amplitude (V_{rf}); B: The time evolution of current amplitude (I_{rf}); C: The time evolution of relative phase φ_{vi} between voltage and current; D: Time evolution of V_{rf}, I_{rf}, and φ_{vi} for the first 15μs for T_1=0μs, 5μs and 10μs; E: The evolution of electron density (n_e) with time in the whole pulse period under different T_1 durations; F: Evolution of power deposition (P_{tot}) and light emission intensity (OEI) with time within the time range of 0μs≤t≤110 μs for different T_1 durations.

after the power turning on, which suggested the occurrence of the ignition. During the post-ignition phase, φ_{vi} increased and all converging to the same steady-state value of 84° during the remaining part of the T_2 phase. After the pulse was turned off, there were significant noises exhibiting in φ_{vi} because the values of V_{rf} and I_{rf} were so small that the calculated φ_{vi} became unreliable at this time. In addition, it was found from Figure 3C that φ_{vi} stayed near 90° prior to the plasma ignition, which indicated that the impedance of the system was purely capacitive at this stage[26,27].

Upon the plasma ignition, I_{rf} exhibited its highest growth rate when V_{rf} experienced a dip, which was accompanied by a rapid decrease in φ_{vi}. Furthermore, the duration of the I_{rf} surge phase gradually became shorter as T_1 increased at the time of V_{rf} showing a dip, suggesting that the ignition became less significant.

For a short linear-rise time of T_1=5μs, the plasma was not yet ignited at the end of the linear rise time that φ_{vi} remained approximately at 90°. The electron energy loss mainly occurred on the electrodes when T_1=10μs, and φ_{vi} dropped to the lowest value then gradually rised during the breakdown stage. During this period, the electron energy

https://doi.org/10.53964/mltp.2023009

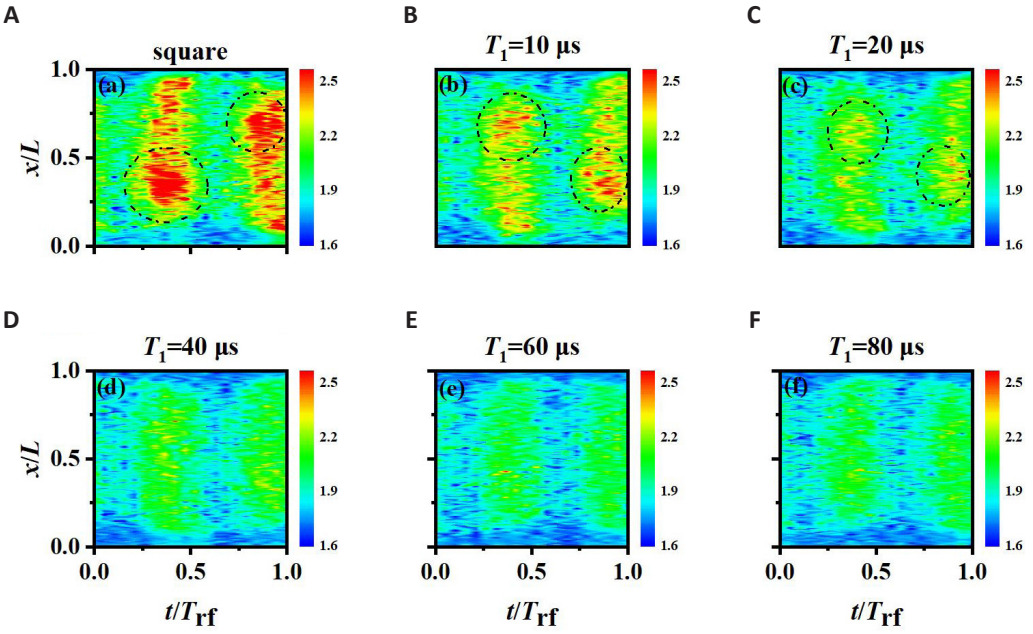

Figure 4. The spatiotemporal distribution of the electron excitation rate in one RF cycle at the time when the light intensity overshoots for different T_1 durations: square(A), 10μs(B), 20μs(C), 40μs(D), 60μs(E), 80μs(F). As the excitation image at T_1=5μs is nearly identical to the square pulse excitation, it is not shown.

loss was related to the electron avalanche process.

For a longer linear-rise time (e.g., T_1≥20μs), the plasma at the end of the linear-rise stage had already been ignited, φ_{vi} kept rising and gradually tended to stabilize. During this time, the sheath has already formed, and the electron energy loss was caused mainly by the collision of electrons with neutral particles in the central region.

The time evolution of the electron density, n_e, during the whole pulse period at different T_1 is shown in semi-logarithmic coordinates in Figure 3E. For each T_1 duration also started to increase rapidly at the time when the power deposition and OEI exhibited the maxima (as Figure 3F) and reached steady-state value of 2×10^{15}cm^{-3} for T_1<80μs, while n_e cannot reach the steady-state value for the T_1=80μs case. Subsequently, after the pulse was turned off, n_e initially experienced a rapid decay with the same rate for different T_1 durations. This initial decay might be caused either by the fast loss of high-energy electrons or by the calibration error of n_e related to the rapidly changing electron temperature[35]. After T_1=125μs, n_e decayed with different rates, corresponding to the loss of medium and low energy electrons. Notably, the decay rate of n_e became lower at a larger T_1 value, and finally reached the lower limit of probe detection. The different decay rates of n_e can be attributed to the fact that longer T_1 duration led to a lower gas temperature and higher neutral gas concentration, therefore the diffusion loss of electrons reduced[36,37].

Figure 3F illustrated the evolution of P_{tot} and the OEI under the same conditions as in Figure 3E. Ptot and the OEI exhibited similar evolution during the plasma ignition process and deviated from each other afterwards. The applied electric field can enter the central region as n_e was very low at the very beginning of each pulse and sheath was not yet established. As a result, the potential primarily dropped across the inter-electrode region, and the power was primarily coupled to the electrons. It can be seen that the overshoot of Ptot and OEI was more significant by reducing the value of T_1, which is consistent with the results that I_{rf} showed faster growth during the ignition with decreasing T_1 duration in Figure 3. For the square wave pulse and T_1=5μs conditions, P_{tot} and the OEI started to decrease after going through their overshoot and gradually reached respective stable values. While T_1 was 10μs or longer, both P_{tot} and the OEI increased and eventually decline to the steady-state values after going through their maxima following the increasing V_{rf}. P_{tot} and the OEI decayed rapidly to zero after the pulse was turned off, while n_e decreased slowly, which was due to the initial rapid loss of high-energy electrons and followed by a relatively slower loss of low-energy electrons[38].

To further understand the high-energy electron excitation dynamics when the OEI overshot, the spatial-temporal evolution of the electron excitation rate within one RF cycle at different T_1 durations were shown in Figure 4. As shown in Figures 4A-C, respectively corresponding to the square-wave pulse, T_1=10μs and T_1=20μs cases, the electron power absorption when the OEI exhibited the maximum was dominated by the "overshoot mode"[22,23]. At this moment, sheath had been not formed and the externally applied electric field can penetrate into the central region and most

of the potential dropped across the central region. In the presence of the high electric field, a region of high positive space charge was gradually formed near the electrode, and the locally enhanced electric field leads to an excitation maximum at the edge of this region of positive space charge. It was worth noting that this excitation maximum diminished with increasing T_1 duration, as indicated by the dashed ellipse in Figure 4E. In contrast, as T_1 increased above 40μs and the excitation at the maximum of the OEI reduced, the "drift" mode[39,40] took over the "overshoot mode" (as Figures 4D-F). Additionally, the similarity of the excitation images for these three conditions further confirmed the findings presented in Figure 3.

4 CONCLUSION

This work presented an investigation about the time evolution of typical electrical parameters and plasma parameters in a RF CCP under a "linear-rise" pulse amplitude modulation. The pulse-on phase of the square pulse was divided into two distinct phases, namely, the "linear rise" (T_1 phase) and "constant" (T_2 phase). The study focused on exploring the impact of varying T_1 duration on the temporal evolution of these parameters.

It was found that at the beginning of each pulse, both V_{rf} and I_{rf} showed a linear increase. Upon the ignition, V_{rf} showed a dip, accompanied by a decrease in φ_{vi} and drastical increase in I_{rf}. Meanwhile, the power deposition and the OEI showed significant overshoot with rapid increase of electron density. The power deposition and the OEI overshoot less significantly as T_1 increased. Except for T_1 = 80μs case, the electron density can reach steady-state after a rapid initial increase. When the power was turned off, the power deposition and the OEI rapidly decay to zero, while the electron density initially decreases with a similar rate for different T_1 durations, which was corresponding to the collisional loss of high-energy electrons. Subsequently, the electron density starts to decay with different rates, primarily attributed to the diffusive loss of medium- and low-energy electrons. The decay rate of the electron density is reduced with increasing T_1 duration, due to lower gas temperature and higher neutral gas density, which suppresses the diffusion loss of electrons.

Compared to the conventional square pulse modulated RF-CCP, the "linear-rise" amplitude modulation approach adds external control knobs to modulate parameters of plasma used for practical material processing. This work presents an experimental investigation in an electropositive gas, and this study is expected to be extended to complex electronegative gases in the future.

Acknowledgments

This work is financially supported by the National Natural Science Foundation of China (Nos. 12275043) and the Fundamental Research Funds for the Central Universities (No. DUT21TD104).

Conflicts of Interest

The authors declared no conflict of interest.

Author Contribution

All authors designed, wrote, and revised the article. All authors approved the final version.

Abbreviation List

CW, Continuous wave
OEI, Optical emission intensity
RF-CCP, Radio frequency capacitively coupled plasma

References

[1] Rossnagel SM, Westwood WD, Haber JJ. Handbook of Plasma Processing Technology. William Andrew: New York, USA, 1991.

[2] Lieberman MA, Lichtenberg AJ. Principles of Plasma Discharges and Materials Processing 2nd edn. New York: Wiley, 2005.

[3] Graves DB. Plasma processing. *IEEE T Plasma Sci*, 1994; 22: 31-42.[DOI]

[4] Kawamura E, Lieberman MA, Lichtenberg AJ. Stochastic heating in single and dual frequency capacitive discharges. *Phys Plasmas*, 2006; 13: 996.[DOI]

[5] Economou DJ. Modeling and simulation of plasma etching reactors for microelectronics. *Thin Solid Films*, 2000; 365: 348-367.[DOI]

[6] Fang Y, Zhang J, Jiang YL. Highly selective etch of silicon dioxide with tungsten hard mask deposited by PVD process: *18th International Workshop on Junction Technology (IWJT)*. Shanghai, China, 2018: 1-3.[DOI]

[7] Suto S, Okano H, Horiike Y. Highly selective etching of Si_3N_4 to SiO_2 employing fluorine and chlorine atoms generated by microwave discharge. *J Electrochem Soc*, 1989; 136: 2032-2034.[DOI]

[8] Volynets V, Barsukov Y, Kim G et al. Highly selective Si_3N_4 / SiO_2 etching using an NF_3 /N_2 /O_2 /H_2 remote plasma. I. Plasma source and critical fluxes. *J Vac Sci Technol A*, 2020; 38: 023007.[DOI]

[9] Huang S, Shim S, Sang KN et al. Pattern dependent profile distortion during plasma etching of high aspect ratio features in SiO_2. *J Vac Sci Technol A*, 2020; 38: 023001.[DOI]

[10] Chen W, Morikawa Y, Itoh M et al. Very uniform and high aspect ratio anisotropy SiO_2 etching process in magnetic neutral loop discharge plasma. *J Vac Sci Technol A*, 1999; 17: 2546-2550.[DOI]

[11] Huang S, Huard C, Shim S et al. Plasma etching of high aspect ratio features in SiO_2 using Ar/C_4F_8 /O_2 mixtures: A computational investigation. *J Vac Sci Technol A*, 2019; 37.[DOI]

[12] Radjenovic BM, Radmanovic-Radjenovic MD, Petrovic ZL. Dynamics of the Profile Charging During SiO_2 Etching in Plasma for High Aspect Ratio Trenches. *IEEE T Plasma Sci*,

2008; 36: 874-875.[DOI]

[13] Zhang P. Study on the Pulse Phase Lag Effect on Two Mask Holes During Plasma Etching. *Braz J Phys*, 2021; 51: 1117-1126.[DOI]

[14] Rauf S, Ba Lakrishna A. SiO_2 etching in an Ar/c-$C4F_8$/O_2 dual frequency capacitively coupled plasma. *J Vac Sci Technol A*, 2017; 35: 021308.[DOI]

[15] Ohmori T, Goto TK, Kitajima T et al. Negative charge injection to a positively charged SiO_2 hole exposed to plasma etching in a pulsed two-frequency capacitively coupled plasma in CF_4/Ar. *Appl Phys Lett*, 2003; 83: 4637-4639.[DOI]

[16] Samukawa S, Mieno T. Pulse-time modulated plasma discharge for highly selective, highly anisotropic, and charge-free etching. *Plasma Sources Sci T*, 1996; 5: 132.[DOI]

[17] Anjum Z, Rehman NU. Temporal evolution of plasma parameters in a pulse-modulated capacitively coupled Ar/O_2 mixture discharge. *Aip Adv*, 2020; 10: 115005.[DOI]

[18] Yuan G, Zhou JQ, Hu MD et al. Pulsed capacitively coupled plasmas for AIO etch process//2016 China Semiconductor Technology International Conference (CSTIC). IEEE, 2016: 1-3.[DOI]

[19] Jang JK, Tak HW, Shin YJ et al. Plasma induced damage reduction of ultra-low-k dielectric by using source pulsed plasma etching for next BEOL interconnect manufacturing. *Ieee T Semiconduct M*, 2020; 33: 302-309.[DOI]

[20] Mishra A, Jeon MH, Kim KN et al. An investigation of the temporal evolution of plasma potential in a 60MHz/2MHz pulsed dual-frequency capacitively coupled discharge. *Plasma Sources Sci T,* 2012; 21: 055006.[DOI]

[21] Sirse N, Jeon MH, Yeom GY et al. Temporal evolution of electron density in a low pressure pulsed two-frequency (60MHz/2MHz) capacitively coupled plasma discharge. *Plasma Sources Sci T*, 2014; 2: 065046.[DOI]

[22] Liu R, Liu Y, Jia W et al. Fluid modeling of plasma dynamics in pulsed RF capacitive glow discharges in low pressure argon. *Phys of Plasmas*, 2017; 24: 083515.[DOI]

[23] Peterson D, Xiao Y, Ford K et al. Electron temperature measurements with a hairpin resonator probe in a pulsed low pressure capacitively coupled plasma. *Plasma Sources Sci T*, 2021; 30: 065018.[DOI]

[24] Cho C, You K, Kim S et al. Characterization of SiO_2 Etching Profiles in Pulse-Modulated Capacitively Coupled Plasmas. *Mater*, 2021; 14: 5036.[DOI]

[25] Hernandez K, Overzet LJ, Goeckner MJ. Electron dynamics during the reignition of pulsed capacitively-coupled radio-frequency discharges. *J Vac Sci Technol B*, 2020; 38: 034005.[DOI]

[26] Liu YX, Wang XY, Zhang QZ et al. Avalanche induced rapid impedance change and electron power absorption during gas breakdown under radio-frequency excitation. *Plasma Sources Sci T*, 2020; 29: 12LT03.[DOI]

[27] Wang XY, Liu JR, Liu YX et al. Comprehensive understanding of the ignition process of a pulsed capacitively coupled radio frequency discharge: the effect of power-off duration. *Plasma Sources Sci T*, 2021; 30: 075011.[DOI]

[28] Su ZX, Shi DH, Liu YX et al. Radially dependent ignition process of a pulsed capacitively coupled RF argon plasma over 300mm-diameter electrodes: multi-fold experimental diagnostics. *Plasma Sources Sci T*, 2021; 30: 125013.[DOI]

[29] Šamara V, Bowden MD, Braithwaite NSJ. Effect of power modulation on properties of pulsed capacitively coupled radiofrequency discharges. *J Phys D Appl Phys*, 2010; 43: 124017.[DOI]

[30] Schulze J, Schüngel E, Donkó Z et al. Phase resolved optical emission spectroscopy: a non-intrusive diagnostic to study electron dynamics in capacitive radio frequency discharges. *J Phys D Appl Phys*, 2010; 43: 124016.[DOI]

[31] Poulose J, Goeckner M, Shannon S et al. Driving frequency fluctuations in pulsed capacitively coupled plasmas. *Eur Phys J D*, 2017; 71: 1-12.[DOI]

[32] Karkari SK, Gaman C, Ellingboe AR et al. A floating hairpin resonance probe technique for measuring time-resolved electron density in pulse discharge. *Meas Sci Technol*, 2007; 18: 2649.[DOI]

[33] Peterson DJ, Ford K, Brandon J et al. Radiofrequency phase resolved electron density measurements with the hairpin resonator probe. *J Phys D Appl Phys*, 2020; 53: 145203.[DOI]

[34] Curley G. The dynamics of the charged particles in a dual frequency capacitively coupled dielectric etch reactor. *Ecole Polytech X*, 2008.[DOI]

[35] Proshina OV, Rakhimova TV, Kovalev AS et al. Experimental and PIC MCC study of electron cooling—re-heating and plasma density decay in low pressure rf ccp argon afterglow. *Plasma Sources Sci T*, 2020; 29: 015015.[DOI]

[36] Han DM, Liu ZG, Liu YX et al. Determination of neutral temperature using fiber Bragg grating sensor in capacitively coupled argon plasmas. *J Appl Phys*, 2016; 119: 113302.[DOI]

[37] Agarwal A, Rauf S, Collins K. Gas heating mechanisms in capacitively coupled plasmas. *Plasma Sources Sci T*, 2012; 21: 055012.[DOI]

[38] Biondi, Manfred A. Diffusion Cooling of Electrons in Ionized Gases. *Phys Rev*, 1954; 93: 1136.[DOI]

[39] Brandt S, Berger B, Schüngel E et al. Electron power absorption dynamics in capacitive radio frequency discharges driven by tailored voltage waveforms in CF4. *Plasma Sources Sci T*, 2016; 25: 045015.[DOI]

[40] Schulze J, Derzsi A, Dittmann K et al. Ionization by Drift and Ambipolar Electric Fields in Electronegative Capacitive Radio Frequency Plasmas. *Phys Rev Lett*, 2011; 107: 275001.[DOI]